

Coupling of spin and lattice modes in the S=1/2 two-dimensional antiferromagnet $K_2V_3O_8$ with magneto-dielectric couplings

K.-Y. Choi,¹ P. Lemmens,² V. P. Gnezdilov,³ B. C. Sales,⁴ and M. D. Lumsden⁴

¹*Department of Physics, Chung-Ang University, 221 Huksuk-Dong, Dongjak-Gu, Seoul 156-756, Republic of Korea*

²*Institute for Physics of Condensed Matter, TU Braunschweig, D-38106 Braunschweig, Germany*

³*B. I. Verkin Institute for Low Temperature Physics NASU, 61164 Kharkov, Ukraine*

⁴*Oak Ridge National Laboratory, P.O. Box 2008, Oak Ridge, Tennessee 37831, USA*

(Dated: August 13, 2018)

Lattice dynamics and magnetic excitations are investigated to elucidate the origin of magneto-dielectric effects in the S=1/2 two-dimensional quantum spin compound $K_2V_3O_8$. We find evidence for lattice instabilities at 110 K and 60 K as optical phonon anomalies and a soft mode at 26 cm^{-1} in A_1 symmetry. Two-magnon excitations in B_1 symmetry show an unconventional double-peak structure and temperature dependence. This suggests the existence of a split mode near the zone boundary caused by a mixing of spin and lattice modes.

I. INTRODUCTION

In recent years, the cross-coupling effects of magnetic and electric properties in a single material have been intensively investigated due to the fascinating underlying physics and the potential to realize multifunctional devices.¹ Prominent examples are found in multiferroic materials such as charge ordered LuFe_2O_4 , magnetically driven RMn_2O_5 (R=rare earth), and lone pair multiferroic compounds $\text{R}(\text{Fe},\text{Mn})\text{O}_3$.²⁻⁴ In such material classes, low-energy excitations are given by so-called electromagnons, which are coupled spin and lattice excitations.⁵ However, it turns out that electromagnons are not a monopoly of the multiferroic materials. Electromagnons have also been observed in the paraelectric phase of a conical-spin magnetically ordered hexaferrite $\text{Ba}_2\text{Mg}_2\text{Fe}_{12}\text{O}_{22}$.⁶

Here the question is to what extent phonon-magnetic coupled modes retain their hybrid nature in nonmultiferroic materials but with magnetodielectric couplings. For such less strongly coupled materials, magnetism is not mutually coupled to ferroelectricity but it is tied to dielectric properties. The $A_2B_3O_8$ fersnoites (A=K,Rb,Cs, NH_4 ; B=Ti, V, Mn, Cu) are suitable for studying the coupling of a soft phonon mode to magnetic excitations because they are susceptible to displace structural phase transition and show novel magnetic properties and non-linear optical properties.⁷⁻¹¹ Actually, magnetodielectric effects have been reported in $K_2V_3O_8$ and are attributed to the interplay between structural and electronic degrees of freedom.¹²

$K_2V_3O_8$ is the S=1/2 square lattice antiferromagnet which has a space group $P4bm$ and lattice parameters $a=8.870 \text{ \AA}$ and $c=5.215 \text{ \AA}$ at room temperature.¹³ The vanadium layer consists of slabs of corner-sharing VO_5 square pyramids and VO_4 tetrahedra, separated by non-magnetic, interstitial K^+ ions.¹⁴ The magnetic behavior is described by a Heisenberg model with an exchange coupling constant of $J = 12.8 \text{ K}$ together with a Dzyaloshinsky-Moriya (DM) interaction and an additional c-axis anisotropy.⁹ The exchange constant is small

because magnetic (S=1/2) $\text{V}^{4+}\text{-O}_5$ pyramids are separated by nonmagnetic (S=0) $\text{V}^{5+}\text{-O}_4$ tetrahedra. Inter-layer couplings and anisotropies lead to an antiferromagnetic ordering at $T_N = 4 \text{ K}$, showing unusual field induced spin reorientations. Magnetization and neutron diffraction studies show continuous spin reorientation in a basal-plane magnetic field.⁹ Theoretical works suggest novel magnetic structures, which consist of chiral helices with rotation of staggered magnetization and oscillations of the total magnetization.^{15,16} Inelastic neutron scattering studies reveal an unexpected mode splitting of a spin wave near the $(\pi/2, \pi/2)$ zone boundary.¹⁷

Thermal conductivity measurements give a hint of a local symmetry breaking as indicated by anomalies around 110 K .¹⁰ Optical spectroscopy measurements confirm a successive structural transition: a distortion of the apical oxygen of the VO_5 square pyramids at about 110 K and a weak basal plane distortion around 60 K .^{7,18} Recent crystallographic measurements unveil a symmetry reduction to space groups $P4_2bc$ or $P4nc$ at 115 K .¹⁹

The most remarkable feature is the observation of magnetodielectric effects by magneto-optical experiments: (i) a redshift of the 1 eV excitation with a vibration fine structure of the frequency 55 cm^{-1} , and (ii) a narrowing of the 2.3 eV excitation with increasing magnetic field.¹² The field-induced changes in the optical excitations were attributed to local distortions of the VO_5 square pyramids with external magnetic field. All these seem to suggest that a soft lattice is coupled to a spin system but clear spectroscopic evidence is missing. Raman spectroscopy can serve as an experimental choice because it is extremely sensitive to both lattice anomalies and low-lying spin excitations.

In this paper, we report on the observation of a soft mode in A_1 symmetry and the two-magnon excitations in B_1 symmetry which show a similar energy scale and temperature dependence. The two-magnon continuum exhibits an unexpected double-peak lineshape. These features are interpreted as resulting from the coupling of spin and lattice modes at finite momentum.

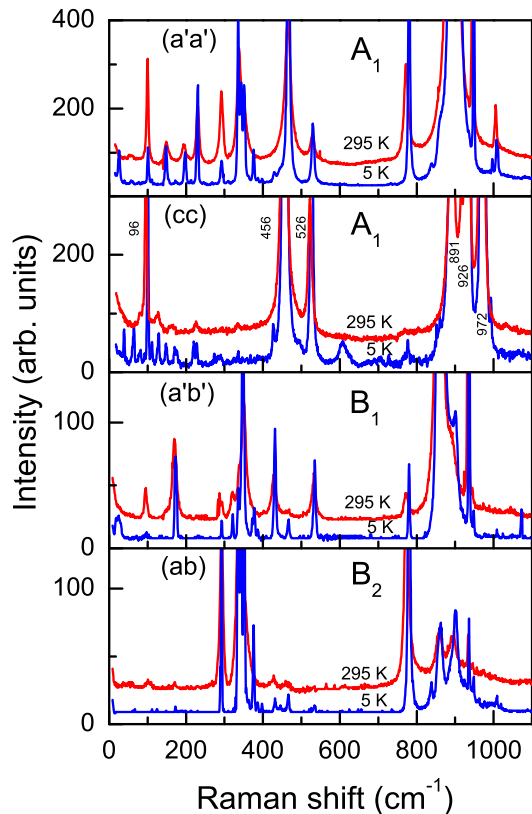


FIG. 1: (Color online) Raman spectra of $\text{K}_2\text{V}_3\text{O}_8$ in four different ($a'a'$), (cc), ($a'b'$), and (ab) polarizations at 5 K and 295 K.

II. EXPERIMENTAL DETAILS

Single crystals of $\text{K}_2\text{V}_3\text{O}_8$ were grown in a platinum crucible by the flux method. Samples with typical dimensions of $4 \times 4 \times 0.1 \text{ mm}^3$ were used for Raman scattering experiments. The Raman spectra were measured in a continuous helium flow optical cryostat by varying temperature from 1.5 K to room temperature. All spectra were taken in a quasi-backscattering geometry with the excitation line $\lambda = 514.5$ of an Ar^+ laser, a DILORXY spectrometer, and a nitrogen cooled charge-coupled device detector. The laser power of 6 mW was focused to a $100 \mu\text{m}$ diameter spot on the crystal.

III. RESULTS AND DISCUSSION

A. Lattice instabilities

Before discussing Raman spectra we present a factor group analysis of the expected phonon modes through the structural transition. At room temperature $\text{K}_2\text{V}_3\text{O}_8$ has a space group $P4bm$ and two formula units ($Z=2$).

The factor group analysis yields the following irreducible representations:

$$\Gamma_{total} = 12A_1(a'a', cc, \mathbf{E}||\mathbf{c}) + 8A_2 + 6B_1(a'b') + 10B_2(ab) + 21E(ac, bc, \mathbf{E}||\mathbf{a}, \mathbf{E}||\mathbf{b}). \quad (1)$$

Here $A_2 + 2E$ modes are acoustic phonon modes.

For temperatures below 115 K a structural transition to space groups $P4_2bc$ or $P4nc$ takes place. For the $P4_2bc$ space group we have the following Γ -point vibrational modes:

$$\Gamma_{total} = 15A_1(a'a', cc, \mathbf{E}||\mathbf{c}) + 15A_2 + 15B_1(a'b') + 15B_2(ab) + 36E(ac, bc, \mathbf{E}||\mathbf{a}, \mathbf{E}||\mathbf{b}). \quad (2)$$

For space group $P4nc$ the total irreducible representations are given as follows:

$$\Gamma_{total} = 15A_1(a'a', cc, \mathbf{E}||\mathbf{c}) + 15A_2 + 13B_1(a'b') + 13B_2(ab) + 32E(ac, bc, \mathbf{E}||\mathbf{a}, \mathbf{E}||\mathbf{b}). \quad (3)$$

In order to discriminate the phonon anomalies induced by the structural phase transition, the Raman spectra were compared at 5 K and 295 K in ($a'a'$), (cc), ($a'b'$), and (ab) polarizations, as shown in Fig. 1. Here $a' = a+b$ and $b' = a-b$ are rotated by 45° from the respective a and b axis. The spectra for the ($a'a'$) and (cc) polarizations consist of A_1 symmetry modes. The crossed ($a'b'$) and (ab) polarizations correspond to the B_1 and B_2 mode, respectively. The E modes which contribute interplane, crossed polarizations could not be studied due to a very thin thickness of the crystal.

At room temperature we observe a total of the $19A_1 + 8B_1 + 8B_2$ modes. The extra $7A_1 + 2B_1$ modes might be due to either local lattice distortions, which activate the silent $7A_2$ modes or a leakage of a selection rule. In contrast, the missing B_2 modes are due to a lack of phonon intensity as well as to their overlap with larger intensity excitations. At $T=3 \text{ K}$ we identify $36A_1 + 14B_1 + 13B_2$. The number of the A_1 modes is much larger than the expected one for both $P4_2bc$ and $P4nc$. The observed B_1 and B_2 modes are not compatible with the space group $P4nc$. This indicates that the real crystal symmetry at 3 K is lower than $P4_2bc$ and $P4nc$ due to an additional base plane distortion at 60 K. Detailed crystallographic characterizations are needed to determine the exact crystal symmetry for temperatures below 60 K.

The vibrational modes are assigned in comparison with the experimental and theoretical Raman works of the vanadium oxides AV_2O_5 ($A=\text{Li, Na, Cs, Mg, Ca}$), which has a similar layered structure consisting of VO_5 square pyramids or VO_4 tetrahedra.^{20–22} The high-frequency modes at $\omega > 500 \text{ cm}^{-1}$ represent the V-O stretching vibrations of the respective VO_4 tetrahedra and VO_5 pyramid. The studied compound has two different V sites and four different O sites: O1(bridging pyramid and tetrahedron), O2(apical to tetrahedron), O3(bridging tetrahedra), and O4(apical to pyramid). Since the bond lengths

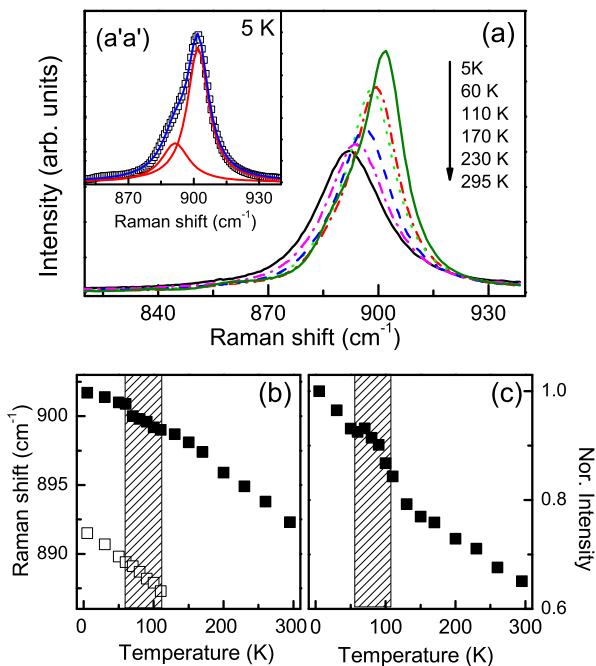


FIG. 2: (a) Temperature dependence of the 891 cm^{-1} mode. Inset: A fit of the 891 cm^{-1} mode to a sum of two Lorentzian curves at 5 K. (b) Temperature dependence of the peak position of the 891 cm^{-1} mode together with a new mode at a shoulder. (c) Temperature dependence of the normalized integrated intensity of the 891 cm^{-1} mode.

of V-O4 and V-O2 are 1.582 and 1.628 \AA , respectively, the highest frequency mode of 972 cm^{-1} observed in the (cc) polarization is the V-O4 stretching mode of the VO_5 square pyramid. The 926 cm^{-1} mode is the V-O2 stretching mode of the VO_4 tetrahedra. The 891 and 526 cm^{-1} modes are the stretching modes of vanadium and basal-plane oxygens. The phonon modes in the frequency range between 200 and 500 cm^{-1} correspond to diverse O-V-O and V-O-V bending vibrations. The low-frequency $\omega < 200\text{ cm}^{-1}$ are assigned to K atom vibrations and torsional and twisting motions of the square pyramids and tetrahedra.

In order to gain local information on lattice distortions through the structural modulation, we highlight the phonon anomalies in the respective low-, intermediate-, and high-frequency regimes. Figure 2(a) shows the temperature dependence of the 891 cm^{-1} mode. At room temperature the peak consists of a single Lorentzian line. Upon cooling through 110 K a new peak shows up at the shoulder of the main peak. The temperature dependence of the frequency exhibits a slight change in

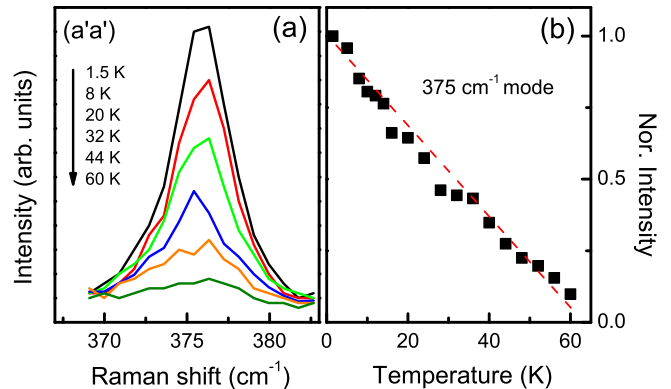


FIG. 3: (a) Evolution of the 375 cm^{-1} peak which appears for temperatures below 60 K . (b) Temperature dependence of the normalized integrated intensity of the 375 cm^{-1} peak. The dashed line is guide for the eyes.

slope around 110 K and a weak jump in the vicinity of 60 K . The normalized integrated intensity also shows anomalies at the respective temperature. The phonon frequency anomalies observed below 110 K are correlated with the dramatic contraction of the a -lattice parameter at the respective temperatures.¹⁹ Here we note that the infrared spectroscopy also observed the splitting of the V-O4 stretching mode for temperatures below 110 K , which was ascribed to the displacement of the apical oxygen from the apex of the VO_5 square pyramid.¹⁸

The Raman scattering intensity is given by the change of a crystal polarizability with respect to the displacements of a normal mode. Dipole matrix elements and interband transition energies are two decisive factors in determining the intensity.²³ Noticeably, the temperature dependence of the 891-cm^{-1} phonon intensity resembles with that of the peak position of the $\text{V}^{4+}d \rightarrow d$ transition [Compare Fig. 6 of Ref. 18 with Fig. 2(c)]. This suggests that local distortions of the VO_5 square pyramids are closely related to electronic properties.

Figure 3 shows the intermediate-frequency mode at 375 cm^{-1} , which is induced by the structural modulations for temperatures below 60 K . Since the new phonon mode corresponds to O-V-O bending vibrations, it results from the basal plane distortions. With decreasing temperature the intensity increases almost linearly without saturation [see Fig. 3(b)]. This indicates that the base plane modulations grow continuously all the way down to the base temperature.

The most striking lattice anomalies are observed in the low-energy phonon modes in (cc) polarization as displayed in Fig. 4. The 95 cm^{-1} mode shows a splitting with decreasing temperature through 110 K . It is remarkable that the infrared-active mode at 55 cm^{-1} also ex-

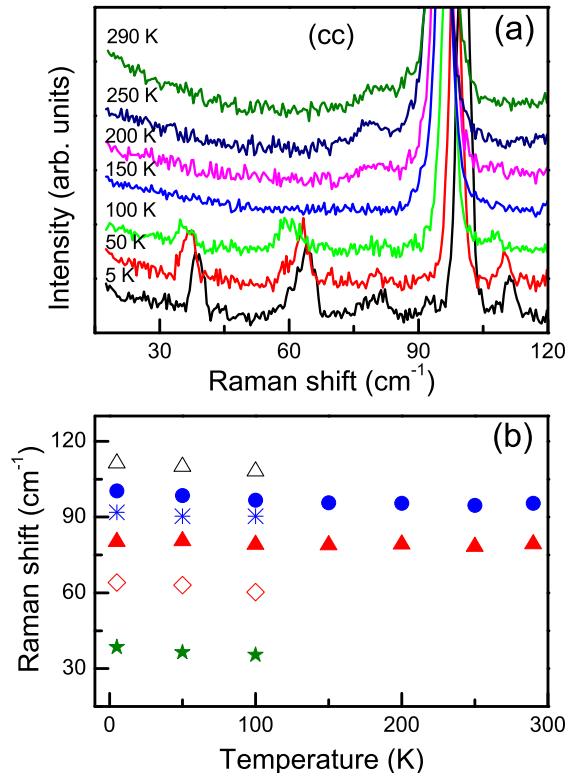


FIG. 4: (Color online) (a) Temperature dependence of the low-frequency Raman spectra in (cc) polarization. (b) Peak splitting of the 95 cm^{-1} mode as a function of temperature.

hibits a similar splitting at the respective temperature.¹² Since these low-frequency modes are associated with the torsional and twisting motions of the square pyramidal and tetrahedral building blocks, the structural modulations are a mixture of out-of-plane bending and rotations of the vanadium oxide polyhedra. We can summarize the evolution of the structural modulations as follows. The rotational modulations of the vanadium oxide polyhedra start around 110 K and then the base plane distortions follow at 60 K. The hardening by 4-5 cm^{-1} indicates that the twisting degree of the V pyramids and the tetrahedra increases substantially upon cooling from 110 K.

B. A soft mode and magnetic excitations

We turn to more direct evidence for a soft lattice. In second-order phase transitions there will always be a zone-center A_1 component of the soft mode below the critical temperature.²⁴ Indeed, we observe the sharp peak at 26 cm^{-1} in the A_1 symmetry as shown in Fig. 5. Upon approaching the phase transition temperature of 60 K the 26 cm^{-1} mode softens and then evolves into quasielastic scattering. We find no evidence for the presence of a

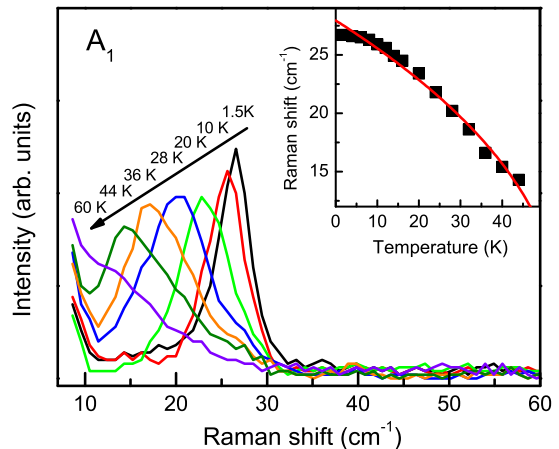


FIG. 5: (Color online) Evolution of the 26- cm^{-1} soft mode in A_1 symmetry which is sensitive to the structural transition at 60 K. Inset: Temperature dependence of the soft mode frequency. The solid line is a fit to a power-law. See the text for details.

Raman-active soft mode related to the structural phase transition at 110 K. The observed soft mode is assigned to the torsional mode that flexes the VO_5 square pyramids out of the plane, which could not be detected by optical spectroscopy.¹² Here we note that the layer compound $\text{SrCu}_2(\text{BO}_3)$ has a soft mode at 62 cm^{-1} as an in-phase motion of almost all ions along an out-of-plane direction.²⁵ This soft mode is a consequence of a continuous corrugation of the Cu-BO_3 layer. This analogy can be taken as further evidence for the basal plane distortions.

The inset of Fig. 5 displays the temperature dependence of the peak position of the soft mode in a temperature range of 1.5 - 45 K. It is well described by a power law, i.e. $\omega = A|T_C - T|^\beta$, with $A = 4.7 \text{ cm}^{-1}/\text{K}$, $T_C = 55 \text{ K}$ and $\beta = 0.448$. The observed critical exponent is close to a mean-field value of $\beta = 1/2$. For $\text{SrCu}_2(\text{BO}_3)$ the soft mode undergoes an additional softening toward low temperatures due to spin-phonon coupling.²⁵ This anomaly is not self-evident for the case of $\text{K}_2\text{V}_3\text{O}_8$ although the small discrepancy between the experimental data and the fitted curve might have an origin of spin-phonon coupling. This is not surprising if the long $\text{V}^{4+}\text{-O-O-V}^{4+}$ superexchange paths are taken into account.

We now switch to the low-energy spin excitation observed in ($a'b'$) polarization. Figure 6(a) compares the magnetic continuum in the B_1 symmetry with the soft mode in the A_1 symmetry. The continuum exhibits a double peak structure extending from 10 cm^{-1} up to 44 cm^{-1} . The primary peak (P1) is centered at 26 cm^{-1} while the secondary peak (P2) lies at 16 cm^{-1} . The primary peak position coincides with the soft phonon mode. The magnetic continuum is ascribed to two-magnon excitations by considering the energy scale of the spectral

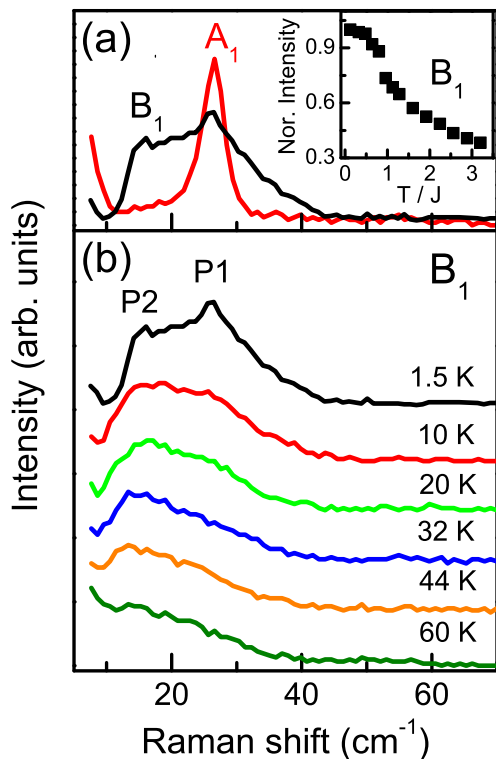


FIG. 6: (Color online) (a) Comparison of the soft mode seen in the A_1 symmetry and the two-magnon continuum observed in the B_1 symmetry. Inset: Temperature dependence of the integrated intensity of two-magnon scattering in a temperature scale of J . (b) Temperature dependence of two-magnon scattering in the B_1 symmetry.

weight and the selection rule (see below).

In two-dimensional (2D) antiferromagnets, two-magnon scattering can be probed as a double spin-flip process via the exchange light scattering.²⁶ A dominant contribution comes from a symmetry-allowed B_1 geometry.²⁷ This selection rule strictly holds for our case. The density of states of a two-magnon spectrum is given by $\rho_2(\omega) = \sum_k \delta(\omega - 2\omega_k)$, where ω_k is a one-magnon dispersion. From the upper cut-off frequency of the two-magnon spectrum, we can determine the magnon energy at the zone boundary. The obtained value of 2.8 meV ($\approx 22.4 \text{ cm}^{-1}$) agrees perfectly with the neutron scattering result (compare to Fig. 12 of Ref.¹⁷).

In addition, we can estimate the exchange coupling constant between vanadium spins by resorting to the upper cut-off relation, that is, $2Z_c JzS = 4.632 J$, where J is the exchange integral, z is the number of nearest neighboring spins, and $Z_c = 1.158$ is a quantum correction to a classical value.^{28,29} We obtain $J \approx 13.6K$. This is in reasonable agreement with the value of $J = 12.8 K$ extracted by inelastic neutron scattering.¹⁷ The small over-

estimation is due to the presence of interlayer interactions and DM interactions. Here we note that a conventional way of determining J from the two-magnon continuum is based on the peak energy, which corresponds to $\omega_p \sim 2.7J$.³⁰ However, this method is not unambiguously applicable to $K_2V_3O_8$ since there is no well-defined single peak unlike other antiferromagnets.^{27,30}

Figure 6(b) shows the temperature dependence of the two-magnon scattering. The spectrum persists to $T=60 K$ in the form of short-range magnetic fluctuations. This temperature amounts to $15 T_N (= 5J)$. The survival of the zone boundary magnon to exceptionally high temperatures in an energy scale of T_N reflects the fact that in 2D $S=1/2$ quantum spin systems magnetic excitations are scaled by an exchange coupling constant J while the classical Néel ordering is caused by interplane interactions. Although the spectral weight of the two-magnon profile matches well with the spin wave theory, a careful inspection of the continuum reveals some anomalies.

First, the relative intensity falls off strongly with an upturn about J [see the inset of Fig. 6(a)]. This behavior is contrasted by other antiferromagnets, which show an increase of a total scattering intensity or a moderate decrease in a high-temperature limit.^{27,30}

Second, the lineshape shows the double-peak structure. Since two-magnon scattering is dominated by zone boundary magnons, it might be due to the zone boundary mode splitting. Indeed, inelastic neutron scattering identifies the split modes at the zone boundary centered around 21 cm^{-1} with an energy difference of 4 cm^{-1} .¹⁷ Since Raman spectroscopy probes magnetic excitations as the two-magnon continuum, the energy difference between the two peaks is expected to double that of the neutron split modes. The observed separation energy of 10 cm^{-1} is slightly larger than twice that of the neutron split modes. Its possible reason is discussed below.

In order to explain the observed split modes Lumsden *et al.*¹⁷ have discussed several possible scenarios, for example, magnon-phonon interaction, structural distortions, lattice disorders, multimagnon scatterings, and orbital degrees of freedom. However, no definite answer can be given. Based on the two-magnon lineshape and temperature dependence, we propose a coupling of a soft mode to magnetic excitations as an origin. The coincidence of the energy scales and temperature dependence makes it difficult to differentiate two modes using experimental techniques different from Raman spectroscopy. Thanks to the Raman selection rules, however, we are able to separate them from each other.

Here we remind the reader that there are soft optical and acoustic modes in structural phase transitions. The former can be observed by Raman spectroscopy while the latter can be detected by Brillouin scattering techniques. Although the dispersion of the soft mode cannot be directly determined by Raman scattering experiments, we can sketch a typical profile by exploiting the fact that the soft optical mode has quite flat dispersion and has a Γ -point energy of 26 cm^{-1} . The resulting dispersion

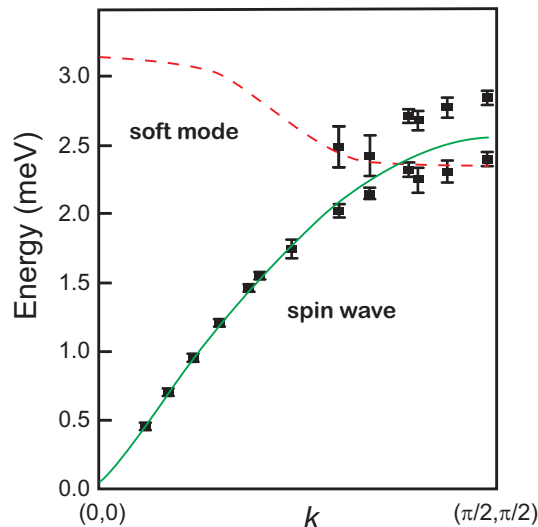


FIG. 7: (Color online) A sketch of coupling of a soft mode to a spin wave near the zone boundary. The spin wave data and their fit to linear spin-wave theory (solid line) are reproduced from Fig. 12 of Ref.¹⁷. The dashed line represents a typical optical dispersion of the soft mode, which is based on the observed Γ -point energy of 26 cm^{-1} .

curve is illustrated schematically as the dashed line in Fig. 7. The soft phonon is presented together with the spin wave obtained by inelastic neutron scattering experiments (squares symbols and solid line in Fig. 7). Judging from the comparable energy scale of the soft mode at the $(0,0)$ point and the magnon at the $(\pi/2, \pi/2)$ point, it is apparent that the soft mode crosses the magnon near the zone boundary. This provides a compelling explanation on the split modes. Since a mixing of the spin and phonon mode occurs near the zone boundary, a coupled spin-phonon character will be manifested at finite momentum. Therefore, we expect no anomalous feature for the Γ -point soft mode as Fig. 5 shows. However, the line-shape and temperature dependence of the two-magnon scattering will be different from conventional antiferromagnets. As Fig. 6 shows, the spectral form and the scattering intensity reflect a hybrid nature.

Last, we detail the anomalous double-peak feature in relation to the neutron split modes. The zone boundary magnons have energies of 19 and 23 cm^{-1} . The corresponding two-magnon density of states has the upper cut-off energies at 38 and 46 cm^{-1} . This energy corresponds to $4.632 J$.^{28,29} Due to magnon-magnon interactions the two-magnon peak is shifted down to $2.7 J$ for 2D antiferromagnets.³⁰ This relation enables us to estimate the peak energies of the two-magnon spectrum as 22 and 27 cm^{-1} . Compared to the observed peak energies of 16 cm^{-1} (P2) and 26 cm^{-1} (P1), only the lower-energy peak shows an appreciable energy difference by 6 cm^{-1} . The discrepancy suggests that there are additional softening channels, specific to the lower-energy branch. This might be due to the fact that the lower branch of the hybrid modes has a more phonon character.

IV. CONCLUSION

To conclude, we have presented Raman scattering studies of $S=1/2$ 2D antiferromagnet $\text{K}_2\text{V}_3\text{O}_8$. Owing to magnetodielectric couplings, this system shows marked anomalies in phonon and magnetic excitations. Successive structural phase transitions at 110 K and 60 K are confirmed by pronounced phonon anomalies in frequencies, intensities, and numbers. Further, for temperatures below 60 K we observe a soft mode at 26 cm^{-1} in A_1 symmetry and two-magnon excitations in B_1 symmetry. The two-magnon continuum shows an unexpected double-peak structure and a pronounced temperature dependence. This is interpreted in terms of a mixing of spin and lattice modes near the zone boundary. Our result suggests that for magnetodielectric materials a mixing of phonon-magnetic modes occurs at finite momentum.

Acknowledgments

This work was supported by NTH and DFG. K.Y.C. acknowledges financial support from the Humboldt Foundation and the NRF of Korea, Grant No. 2009-0093817.

¹ S.-W. Cheong and M. Mostovoy, *Nat. Mater.* **6** 13, (2007).

² J. Wang, J. B. Neaton, H. Zheng, V. Nagarajan, S. B. Ogale, B. Liu, D. Viehland, V. Vaithyanathan, D. G. Schlom, U. V. Waghmare, N. A. Spaldin, K. M. Rabe, M. Wuttig, and R. Ramesh, *Science* **299**, 1719 (2003).

³ T. Kimura, T. Goto, H. Shintani, K. Ishizaka, T. Arima, and Y. Tokura, *Nature (London)* **426**, 55 (2003).

⁴ N. Hur, S. Park, P. A. Sharma, J. S. Ahn, S. Guha, and S.-W. Cheong, *Nature (London)* **429**, 392 (2004).

⁵ M. Kenzelmann, *Physics* **4**, 88 (2011).

⁶ N. Kida, D. Okuyama, S. Ishiwata, Y. Taguchi, R. Shimanu, K. Iwasa, T. Arima, and Y. Tokura, *Phys. Rev B* **80**, 220406 (2009).

⁷ R. L. Withers, T. Höche, Y. Liu, S. Esmailzadeh, R. Keding, B. C. Sales, *J. Solid State Chem.* **177**, 3316 (2004).

⁸ T. Höche, W. Neumann, S. Esmailzadeh, R. Uecker, M. Lentzen, C. Russel, *J. Solid State Chem.* **166**, 15 (2002).

⁹ M. D. Lumsden, B. C. Sales, D. Mandrus, S. E. Nagler, and J. R. Thompson, *Phys. Rev. Lett.* **86**, 159 (2001).

¹⁰ B. C. Sales, M. D. Lumsden, S. E. Nagler, D. Mandrus, and R. Jin, *Phys. Rev. Lett.* **88**, 095901 (2002).

¹¹ J. K. Yuan, P. Z. Fu, J. X. Wang, F. Guo, Z. P. Yang, Y. C. Wu, *Prog. Cryst. Growth Character. Mater.* **40**, 103 (2000).

¹² R. C. Rai, J. Cao, J. L. Musfeldt, D. J. Singh, X. Wei, R. Jin, Z. X. Zhou, B. C. Sales, and D. Mandrus, *Phys. Rev.*

- B **73**, 075112 (2006).
- ¹³ J. Galy and A. Carpy, *Acta Crystallogr., Sect. B : Struct. Crystallogr. Cryst. Chem.* **31**, 1794 (1975).
- ¹⁴ G. Liu, J. E. Greedan, *J. Solid State Chem.* **114** 499-505 (1995).
- ¹⁵ A. N. Bogdanov, U. K. Rossler, M. Wolf, K. H. Muller, *Phys. Rev. B* **66**, 214410 (2002).
- ¹⁶ A. L. Chernyshev, *Phys. Rev. B* **72**, 174414 (2005).
- ¹⁷ M. D. Lumsden, S. E. Nagler, B. C. Sales, D. A. Tennant, D. F. McMorrow, S.-H. Lee, and S. Park, *Phys. Rev. B* **74**, 214424 (2006).
- ¹⁸ J. Choi, Z. T. Zhu, J. L. Musfeldt, G. Raghianti, D. Mandrus, B. C. Sales, and J. R. Thompson, *Phys. Rev. B* **65**, 054101 (2001).
- ¹⁹ B. C. Chakoumakos, R. Custelcean, T. Kamiyama, K. Oikawa, B. C. Sales, M. D. Lumsden, *J. Solid State Chem.* **180** 812 (2007).
- ²⁰ Z. V. Popovic, R. Gajic, M. J. Konstantinovic, R. Provoost, V. V. Moshchalkov, A. N. Vasil'ev, M. Isobe, and Y. Ueda, *Phys. Rev. B* **61**, 11454 (2000).
- ²¹ Z. V. Popovic, M. J. Konstantinovic, R. Gajic, V. N. Popov, M. Isobe, Y. Ueda, and V. V. Moshchalkov, *Phys. Rev. B* **65**, 184303 (2002).
- ²² J. Spitaler, E. Ya. Sherman, H. G. Evertz, and C. Ambrosch-Draxl, *Phys. Rev. B* **70**, 125107 (2004).
- ²³ E. Ya. Sherman, O. V. Misochko, and P. Lemmens, in *Spectroscopy of High- T_c Superconductors*, edited by N. M. Plakida (Taylor & Francis, London 2003), pp. 97-158.
- ²⁴ J. M. Worlock, *Bull. Am. Phys. Soc.* **14**, 368 (1969).
- ²⁵ K.-Y. Choi, Yu. G. Pashkevich, K. V. Lamonova, H. Kageyama, Y. Ueda, and P. Lemmens, *Phys. Rev. B* **68**, 104418 (2003); K. Sparta, G.J. Redhammer, P. Rousssel, G. Heeger, G. Roth, P. Lemmens, A. Ionescu, M. Grove, G. Gntherodt, F. Hning, H. Lueken, H. Kageyama, K. Onizuka, Y. Ueda, *Euro. Phys. Journ. B* **19**, 507-516 (2001).
- ²⁶ P.A. Fleury, and R. Loudon, *Phys. Rev.* **166**, 514 (1968).
- ²⁷ K.-Y. Choi, P. Lemmens, D. Heydhausen, G. Guntherodt, C. Baumann, R. Klingeler, P. Reutler, and B. Buchner, *Phys. Rev. B* **77**, 064415 (2008).
- ²⁸ J. I. Igarashi, *Phys. Rev. B* **46**, 10763 (1992).
- ²⁹ R. R. P. Singh and M. P. Gelfand, *Phys. Rev. B* **52**, R15695 (1995).
- ³⁰ M.G. Cottam and D.J. Lockwood, *Light Scattering in Magnetic Solids*, John Wiley & Sons (1986).